IOSR Journal of Applied Chemistry (IOSR-JAC)
e-ISSN: 2278-5736.Volume 19, Issue 5 Ser. I (May. 2026), PP 21-31
www.iosrjournals.org

Visible-Light-Driven Photocatalytic Remediation Of Organic Pollutants Using A Novel Bimetallic Cu (II) Complex Integrated With A Pyrazine-Based Tetradentate Ligand: Synthesis, Characterization, And Mechanistic Insights

Venkatesh Gaddameedi, Venkateshwar Rao D. And Someshwar Pola
Department Of Chemistry, Osmania University, Hyderabad, Telangana, India

Abstract:
In this context, the construction of efficient, stable and visible-light-active photocatalysts lies at the heart of sustainable wastewater treatment. Herein, we report on the rational design and synthesis of a new tetradentate ligand, 2,2'-(pyrazine-2,5-diyl)bis(4,5-dichlorophenol) (DPPD), and corresponding bimetallic Cu(II) complex, [Cu_2(DPPD)(OAc)2(H2O)2]. The structural integrity of species was validated in detail via 1H/13C-NMR, FTIR, and High-Resolution Mass Spectrometry (HRMS). Optical analysis showed a substantial bandgap narrowing from 2.58 eV to 1.43 eV (ligand and complex) in optical studies as a result, leading to remarkable visible light harvesting. Conventional electrochemical investigations (CV and EIS) showed the availability of accessible Cu(II)/Cu(I) redox couples and a decrease in charge transfer resistance after metalation in the reaction process, as compared to metalification. The complex revealed excellent overall photo catalytical properties, reducing cationic (Methylene Blue (MB), Methyl Violet (MV)) and anionic (Congo Red (CR), Methyl Red (MR)) dyes, which also showed complete degradability around 99 percent at 75 min in 75 minutes of irradiation. The kinetic modelling indicated the pseudo-first order mechanism, with Methylene Blue having the highest rate constant (k = 0.0939 min-1). The scavenger studies indicated photogenerated holes (h^+) and hydroxyl radicals ($^{\bullet}OH$) as the main reactive oxygen species. In addition, the complex showed excellent reuse over six cycles (>99% efficiency) and robust strength in structure, as observed in post-catalytic ESR spectrograms. This study presents [Cu_2(DPPD)] as a strong, stable, and flexible candidate for the mineralization of persistent organic pollutants.

Date of Submission: 06-05-2026 Date of Acceptance: 16-05-2026

I. Introduction:

Under the rapid intensification of industrialization, especially in fabric, paper and plastic industries, significant global water crises have emerged which is attributed to the release of persistent organic pollutants (POPs) into aquatic waters.[1-3] Organic dyes constitute a considerable percentage of these impurities where approximately 15% of the global production of dyes is wasted during the dyeing and spilled in effluent. These dyes are typically complex and have high stability in chemicals which make them resistant to biological and physical treatments for conventional purposes. The inclusion of these pollutants in water not only affects the aesthetic quality of the solution but also inhibits the penetration of light, affecting photosynthetic activities and causing a carcinogenic and mutagenic hazard to the life and the human populations in the water. Therefore, it is an urgent call to develop advanced oxidation processes (AOPs)[4] to mineralize the pollutants completely into non-toxic ones like CO_2 and H_2O.[5]

Of these available AOPs, heterogeneous photocatalysis has been identified as an environmentally benign and economical approach for wastewater remediation.6-8 Traditional semiconductor photocatalysts, mainly TiO_2, are well-studied for stability and toxicity.[9] With their broad bandgaps (usually >3.0 eV), however, their activity is usually limited to the ultraviolet region, which covers < 5% of this region's solar light.10 In trying to harness what is really such a large amount of visible radiation (about 45% of our energy), researchers have tried various ways: doping agents which produce hetero junctioning species for instance.[11-12] Molecular photocatalysts can therefore make use of the benefits of ligand design in order to tailor electronic as well as steric properties to be beneficial, including light absorption, redox potentials, and where to locate a site of activity. In recent years, bimetallic complexes have received a lot of attention in the field of catalysis. The combination of two metal centres in close localities will normally result in a favourable synergistic effect, which is limited or absent in mononuclear analogs.[13-15] Such favourable effects consist of the following: improved charge transfer activity, the

separation of e-/h+ pairs, and a multi-electron redox process. Copper, as a first-row transition metal, is very attractive because of higher abundance, lower toxicity, and versatile nature in Cu^{2+}/Cu^{+} redox chemistry. The coupling of copper to a hard, conjugated structure would support stable structures, which in turn would allow reactive oxygen species (ROS) production under visible light.[16-18]

Ligand selection is key to the stability and catalytic effectiveness of the metal complex.[19] Herein, we study a tetradentate system based on pyrazine. The strong electron-withdrawing bridge formed by the pyrazine moiety allows for this conjugated electronic signalling pathway between metal centres. The additions of phenolic units offer hard oxygen donors to bind Cu(II) ions within an efficient coupling on deprotonation. In addition, adding chlorine substituents to the phenol rings is a valuable design decision; the electron-withdrawing property of the chlorine atoms can manipulate the redox potential of the metal centre and, consequently, also could stabilize the complex towards oxidative degradations.[20]

In this study, we provide the synthesis of 2,2'-(pyrazine-2,5-diyl)bis(4,5-dichlorophenol) (DPPD) and its di copper complex with reference to the principles of bimetallic synergy and conjugated ligand construction. Our main goal is to show that, the combination of the DPPD ligand with Cu(II) provides a photocatalyst with a much narrower bandgap and excellent charge transfer capability. To explore the molecular architecture, we introduce a detailed characterization tool set, composed of NMR, HRMS, FTIR, and ESR, as well. In addition, we test the "universal" catalytic activity capability of the complex to various dyes and carry out kinetic modelling, and radical trapping experiments to offer a conclusive mechanistic characterization of degradation mechanism.

Experimental Part:
Scheme:

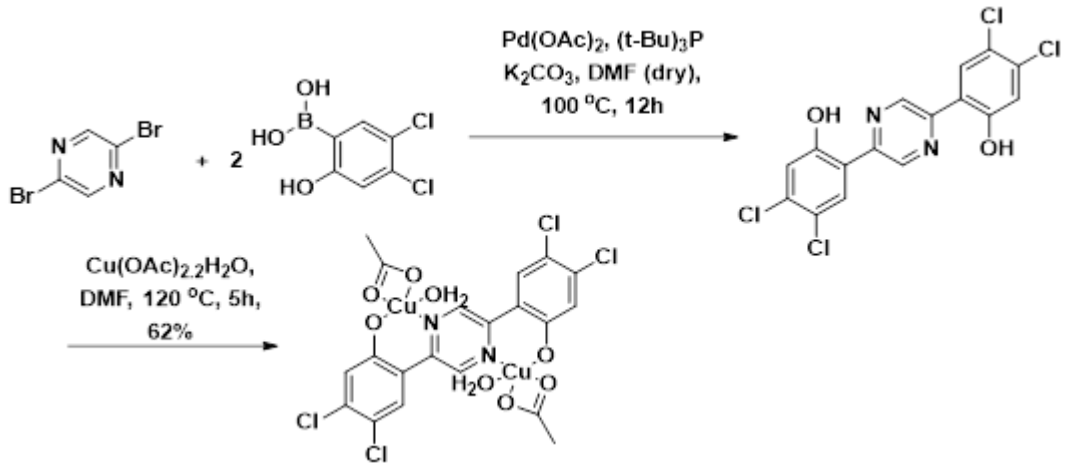

Synthesis of 2,2'-(pyrazine-2,5-diyl)bis(4,5-dichlorophenol)

All reactions were performed in oven-dried glassware under an atmosphere of dry argon using standard Schlenk techniques. 2,5-Dibromopyrazine, $Pd(OAc)_2$, tri-tert-butyl phosphine ($(t\text{-}Bu)_3P$, 10% solution in toluene), and anhydrous N,N-dimethylformamide (DMF) were purchased from Sigma-Aldrich and used as received. (4,5-Dichloro-2-hydroxyphenyl) boronic acid was purchased from Synocule Research labs, Hyderabad, Telangana, India. All other reagents were purchased from commercial suppliers and used as received and directly used.

*Experimental detail***:** To a 50 mL Schlenk flask equipped with a magnetic stir bar were added 2,5-dibromopyrazine (1.0 equiv, 238 mg, 1.0 mmol), (4,5-dichloro-2-hydroxyphenyl) boronic acid (2.2 equiv, 455 mg, 2.2 mmol), potassium carbonate (K_2CO_3, 4.0 equiv, 552 mg, 4.0 mmol), and $Pd(OAc)_2$ (5 mol%, 11 mg, 0.05 mmol). The flask was evacuated and backfilled with argon three times. A solution of $(t\text{-}Bu)_3P$ (10 mol%, 0.10 mmol, 10% solution in toluene) in anhydrous DMF (10 mL) was added via syringe.

The resulting mixture was degassed via three freeze-pump-thaw cycles. The reaction vessel was then placed in a pre-heated oil bath at 100 °C and stirred for 12 h. The progress of the reaction was monitored by thin-layer chromatography (TLC). Upon completion, the reaction mixture was cooled to room temperature and diluted with ethyl acetate (30 mL). The mixture was filtered through a short pad of Celite to remove palladium species and inorganic salts, washing the pad thoroughly with additional ethyl acetate. The filtrate was washed with water (3 x 20 mL) and brine (20 mL). The organic layer was dried over anhydrous Na_2SO_4, filtered, and concentrated under reduced pressure. The crude residue was purified by flash column chromatography on silica gel (using a gradient of petroleum ether/ethyl acetate) to afford the title compound as a dark yellow solid.

Analytical Data: Yield: 73%.

Synthesis of $[Cu_2(DPPD)(OAc)_2(H_2O)_2]$:

The synthesis of the bimetallic Cu (II) complex was carried out by coordinating the tetradentate DPPD ligand with Cu(II) acetate dihydrate in a 1:2 molar ratio.

To a 50 mL round-bottom flask equipped with a magnetic stir bar and a reflux condenser, the synthesized DPPD ligand (1.0 equiv., 400 mg, 1.0 mmol) was dissolved in anhydrous N,N-dimethylformamide (DMF, 15 mL). To this stirring solution, Cu (II) acetate dihydrate $[Cu(OAc)_2.2H_2O]$ (2.2 equiv., 439 mg, 2.2 mmol) was added in one portion. The reaction mixture was heated to 120 °C in a pre-heated oil bath and stirred vigorously for 5 hours. The colour of the solution gradually transitioned from yellow to a deep brownish-green, indicating the formation of the bimetallic complex. The progress of the coordination was monitored by TLC and the disappearance of the free ligand's characteristic fluorescence under UV light. After 5 hours, the reaction mixture was allowed to cool to room temperature. The complex was precipitated by the slow addition of cold distilled water (30 mL). The resulting solid was collected by vacuum filtration and washed thoroughly with cold water (3 x 10 mL) followed by chilled ethanol (2 x 5 mL) to remove unreacted copper salts and residual DMF. The crude product was recrystallized from a mixture of DMF and methanol to afford the pure $[Cu_2(DPPD)]$ complex as a microcrystalline solid.

Analytical Data: **Yield**: 62% (420 mg); dark brownish-green solid; soluble in DMF and DMSO; sparingly soluble in $CHCl_3$ and CH_3OH and *HRMS (ESI+):* m/z calculated for $[C_{20}H_{17}Cl_4Cu_2N_2O_8]^+$ ($[M+H]^+$) = 678.8331; Found: 678.8259.

II. Results & Discussion:

1H-NMR spectroscopy in CDCl3 confirmed the structural integrity and symmetry of the tetradentate ligand DPPD, which exhibited four distinct sets of signals consistent with its Ci molecular symmetry. A pronounced singlet at δ 9.567 ppm is assigned to the phenolic hydroxyl protons (H_a), whose downfield shift implies the formation of intramolecular hydrogen bonding with the pyrazine nitrogen atoms that pre-arranges the ligand for metal coordination.[21] The pyrazine core protons (H_b) show a singlet at δ 8.236 ppm, the characteristic result of the electron-deficient diazine ring. The aromatic protons of the 4,5-dichlorophenol moieties are resolved as two singlets at δ 7.911 ppm (H_c) and δ 7.567 ppm (Hd); the lack of vicinal coupling (3J) between these protons confirms their para orientation relative to one another, verifying the 4,5-dichloro substitution pattern on the 1,2-disubstituted phenolic rings. Residual solvent (δ 7.26 ppm) and water (δ 1.58 ppm) peaks were also noted, with the integration ratios (1:1:1:1 for the primary signals) perfectly matched with the proposed symmetric structure.[22]

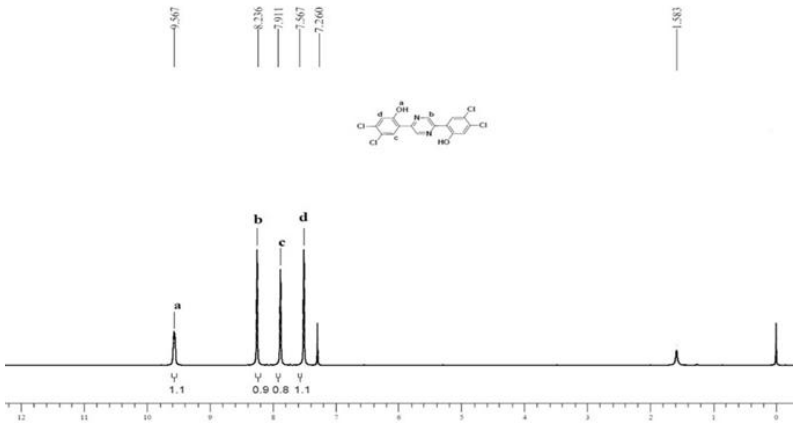

Figure 1 ^{1}H-NMR spectrum of DPPD ligand.

The DPPD ligand's structural framework was further validated by 13C-NMR spectroscopy in CDCl3, which revealed eight unique carbon signals that correspond to the highly symmetric Ci molecular environment. The most downfield signal at δ 156.51 ppm belonged to the phenolic carbon (C-OH), while the substituted pyrazine carbons at δ 154.74 ppm confirm the successful linkage between the aryl and heterocyclic rings.[23] The presence of the pyrazine methine carbons is verified by the signal at δ 140.40 ppm. In dichlorophenolic rings, the quaternary carbons bearing the chlorine atoms present at δ 129.88 ppm and 129.37 ppm indicate the electronegative influence of the halogen substituents. The bridgehead aromatic carbon linked to the pyrazine ring lies at δ 127.39 ppm, and the two-remaining aromatic methine carbons are resolved at δ 119.87 ppm and 115.17 ppm. The characteristic triplet of the CDCl3 solvent is cantered at δ 77.16 ppm. No extraneous signals can be detected, and such well-resolved carbon distribution confirms the high purity of the synthesized ligand and the exact 2,5-pyrazine and 4,5-dichlorophenol substitution patterns of this product.

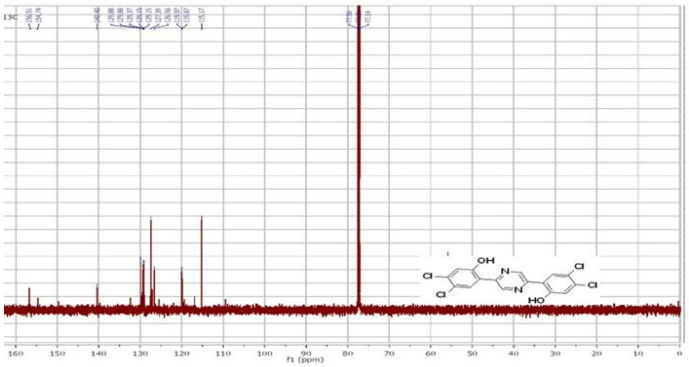

Figure 2 ^{13}C-NMR spectrum of DPPD ligand.

High-Resolution Mass Spectrometry (HRMS) confirmed the molecular formula of the synthesized tetradentate ligand DPPD. The spectrum has a prominent base peak at m/z: 401.0036, which corresponds to the protonated molecular ion $[M+H]^+$ (calculated for $C_{16}H_9Cl_4N_2O_2$: 400.9413). This obtained value is well within the allowable error zone for high resolution (Mw = 399.9341) for molecular weight. Besides, the peak at m/z: 401.0036, the primary isotope peak of the characteristic isotopic cluster created by four chlorine atoms in the molecular structure, is also visible. Relative intensities and distances of the surrounding peaks (m/z: 401–407) correlate with the theoretical M, M+2, M+4, M+6, and M+8 distribution expected for a tetra chlorinated species, further confirming the effective addition of the 4,5-dichlorophenol moieties onto the pyrazine core.

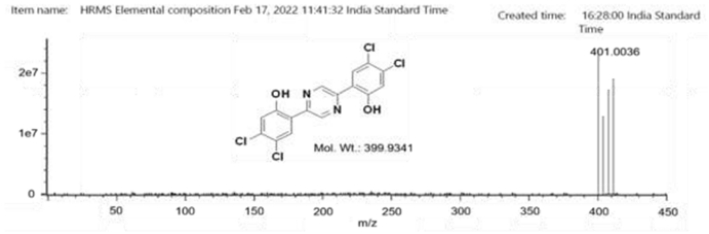

Figure 3 HRMS spectra of DPPD ligand.

The ESI+ characteristic value of the [Cu2(DPPD)(OAc)2(H2O)2] complex can unequivocally support its bimetallic molecular composition. The peak observed at m/z 678.8259 coincides directly with the protonated molecular ion [M + H]+ (calculated for $C_{20}H_{17}Cl_4Cu_2N_2O_8$: 678.8331), and shows barely deviation from the theoretical molecular weight of 677.8253. One of the most vital characteristics of the spectrum is the highly characteristic isotopic manifold in the m/z 678–688 range, whose complex overlapping patterns form an exact signature that has been predicted to resemble the theoretical distribution of the two copper atoms (^{63}Cu and ^{65}Cu) and four chlorine atoms (^{35}Cl and ^{37}Cl), for the tetra chlorinated Di copper framework. The high intensity of the molecular ion peak and the lack of major dissociation products confirm the exceptional stability of the neutral bimetallic construction where DPPD ligands are joined by two acetate and two aqua ligands as they fulfil the coordination demands of the copper centres.[24]

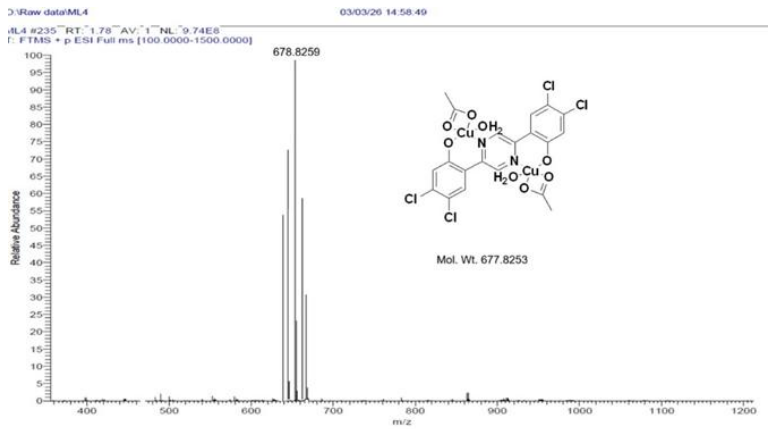

Figure 4 HRMS spectrum of [Cu_2(DPPD)] complex.

The photophysical properties of the DPPD ligand and its [Cu2(DPPD)] complex were examined with UV-Vis absorption and photoluminescence (PL) spectroscopy (as seen in Figures 5a and 5b). The free DPPD ligand (Figure 5a) demonstrates a primary electronic transition in the ultraviolet region centred at approximately 330 nm, where π→π* transitions are observed in the aromatic and pyrazine frameworks, resulting in an optical bandgap (Eg) of 2.58 eV.[25] According to these spectra, upon complexation with Cu(II) ions, a large bathochromic shift is observed in the absorption profile of [Cu2(DPPD)], including a broad, multi-featured band extending into the visible and near-infrared regions (400–800 nm). This shift results in a substantially narrowed bandgap of 1.43 eV, due to both metal-to-ligand charge transfer (MLCT) and ligand-to-metal charge transfer (LMCT) processes, together with the distorted d-d transitions that are typical of the Di copper center.[26-27]

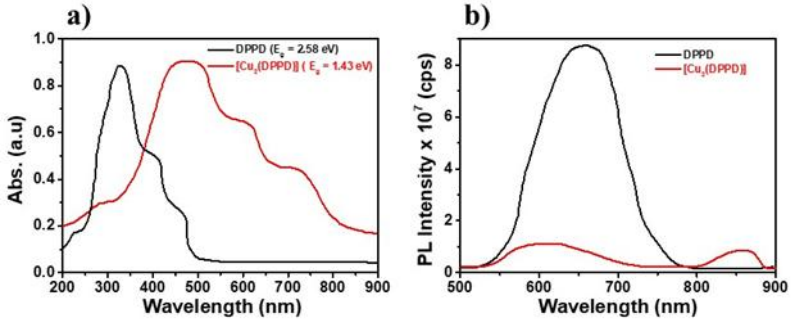

Figure 5 a) UV-vis spectra, and b) PL spectra of ligand DPPD, and [Cu_2(DPPD)] complex.

These shifts are reflected in the PL spectra (Figure 5b) where the strong emission peak of the free ligand lies around 660 nm while the [Cu_2(DPPD)] complex has a dramatic dip in this fluorescence intensity. As a result of this, the Cu^{2+} ions turn off the fluorescence, which is due to its paramagnetic nature and also to the presence of non-radiative relaxation paths between the metal-ligand vibrational modes. Curiously, the complex exhibits a novel weak emission feature in the near-infrared region (860 nm), perhaps indicating a distinct excited-state manifold, likely due to a unique bimetallic architecture.

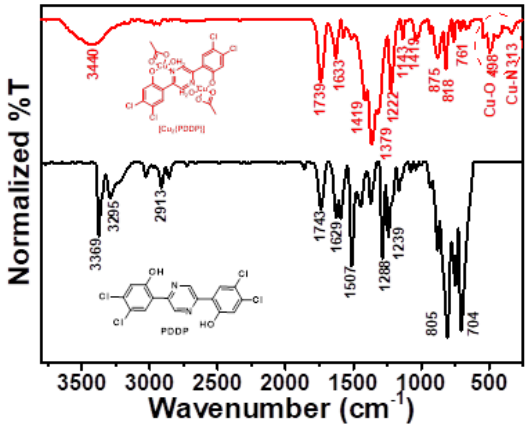

Figure 6 FTIR spectra of both ligand DPPD and [Cu_2(DPPD)] complex.

In the free ligand spectrum, sharp absorption bands at 3369 and 3295 cm^{-1} are ascribed to the stretching vibrations of phenolic O-H atoms; their replacement by a broad envelope at 3440 cm^{-1} in the [Cu2(DPPD)] complex signifies the deprotonation of the phenol groups and their subsequent coordination to the metal ions, likely accompanied by associated water molecules.[28,29] The characteristic stretching frequency -C=N of the pyrazine ring of the ligands at 1629 cm^{-1} shifts to 1633 cm^{-1} of the complex which proves that pyrazine nitrogen atoms were important members of the chelation chain.[29] The marked change and movement of the stretching vibration of phenolic C-O from 1288 cm^{-1} in the ligand to 1222 cm^{-1} in the complex also is indicative of oxygen-dependent bonding. Importantly, the addition of two novel vibrational bands in the far-IR regions at 498 cm^{-1} and 313 cm^{-1} is determined as for the formation of Cu-O and Cu-N bonds, respectively, evidencing that the bimetallic tetradentate structure has assembled successfully.[30]

Electrochemical Properties of DPPD and [Cu_2(DPPD)] Complex:

The electrochemical behaviour and charge-transfer kinetics of the DPPD ligand and its [Cu_2(DPPD)] complex were investigated with cyclic voltammetry (CV) and electrochemical impedance spectroscopy (EIS); these results are presented in Figures 7a and 7b, with the cyclic voltammogram (Fig. 7a) recorded in the potential range between -2.0 V and +2.0 V (vs. Ag/AgCl) showing clear redox signatures for both species. The free DPPD ligand (black trace) displays a quasi-reversible redox pair with a cathodic peak (E_{pc}) at −1.23 V and anodic peak (E_{pa}) around −0.85 V, attributed to the reduction and the consequent re-oxidation of the pyrazine-based compound. As the copper complex, the [Cu_2(DPPD)] complex (red trace) exhibits the occurrence of intense anodic shift along with the appearance of new redox features.[31] E_{pc} = -0.23 V and E_{pa} = -0.61 V represent a powerful redox couple typical of the Cu(II)/Cu(I) redox in the bimetallic center. Additionally, a second reduction peak occurs at around -1.76 V (E_{pc}), with an associated oxidation at -1.25 V (E_{pa}), indicating either the consecutive reduction of the two copper centres or an altered metal surrounding ligand-centred reduction. Shifting in peak potentials, increase in the current response of the complex is suggestive of enhanced electron sharing between the metal centres and the conjugated tetradentate ligand.[32]

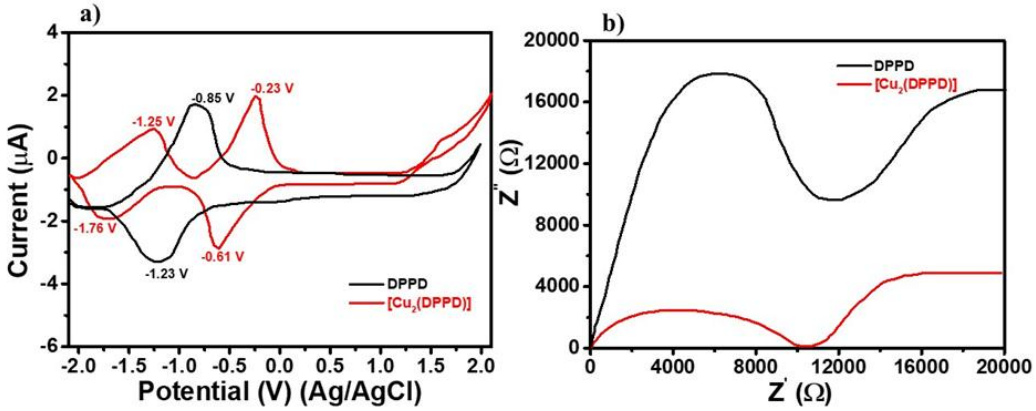

Figure 7 a) Cyclic volta grams, and b) EIS spectra of the ligand DPPD and [Cu_2(DPPD)] complex.

The charge-transfer properties were also analysed again using EIS (Figure 7b), displayed as Nyquist plots. Both the ligand and the complex display characteristic semi-circular arcs in the high-frequency region, representing the charge-transfer resistance (Rct) at the electrode-electrolyte interface.[32] The free DPPD ligand has a much larger semi-circle diameter which suggests a very high resistance to the electron transfer. In contrast, the [Cu_2(DPPD)] complex displays a significant decrease in the arc diameter. The significant reduction with respect to the R_{ct} indicates that the addition of Cu (II) ions into the ligand framework leads to a notable improvement of electrical conductivity and faster interfacial charge transfer kinetics.[33] This increased conductivity agrees well with the smaller optical bandgap found in UV-Vis experiments and highlights the potential of the [Cu_2(DPPD)] complex for applications in photocatalysis.

Photocatalysis:

Photocatalytic Degradation of Organic Dyes by [Cu_2(DPPD)]:

The photocatalytic performance of the [Cu2(DPPD)] complex was investigated by assessing the degradation of the cationic and anionic organic dyes under light irradiation. The time-dependent UV-Vis absorption spectra of Methylene Blue (MB), Methyl Violet (MV), Congo Red (CR), and Methyl Red (MR)[34-37] by the catalyst were depicted in Figures (6a–6d). See for example the characteristic absorption peaks for MB (λmax: 664 nm) and MV (λmax: 584 nm) indicated in Figures 8a and 8b, which are rapidly and significantly reduced in intensity after 75 min. Methylene Blue showed absorption close enough to the baseline value after 75 minutes irradiation, indicating almost complete degradation. The same phenomena can be seen for Methyl Violet, where the large peak at 584 nm gradually decreases. A dark adsorption period (-30 min to 0 min) indicates a prominent decrease in absorbance, which indicates that the [Cu2(DPPD)] complex also has strong adsorption for cationic species, presumably due to electron-rich pyrazine and phenolic oxygen sites on the surface of the catalyst.

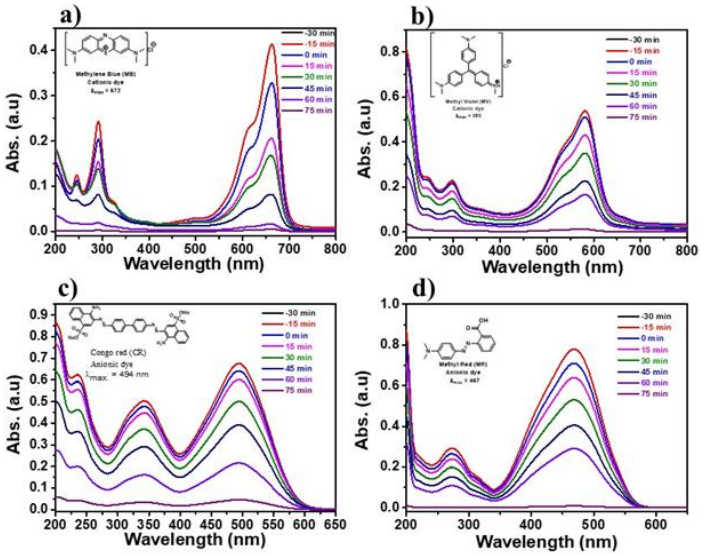

Figure 8 Temporal changes of UV-vis spectra of a) MB, b) CV, c) CR, and d) MR dyes in the presence of [Cu_2(DPPD)] complex.

In the same way, the catalytic activity extended to anionic dyes congo red (CR) and methyl red (MR) seen as shown in Figures 8c and 8d. CR (494 nm) and MR (467 nm) present efficient degradation. The consistent decrease in absorbance, without new peaks in the visible region, indicates that the chromophore structures were completely mineralized or broken down rather than transformed into intermediate colors.[38] The [Cu_2(DPPD)] complex possesses versatile universal photocatalytic properties, efficiently cleaving both cationic and anionic dyes. This efficiency is due to the following reasons: (i) narrow bandgap: The previous established optical bandgap of 1.43 eV allows for efficient visible-light harvesting and the generation of electron-hole (e^-/h+) pairs (ii) redox function: The CV data proved the existence of accessible Cu(II)/Cu(I) redox couples, which are important in promoting electron transfer to the dissolved oxygen to result in the superoxide radicals ($O_2^{-\bullet}$) or hole trapping by water to form hydroxyl radicals ($^\bullet$OH); (iii) bimetallic coupling : The dicopper center is able to promote charge carrier separation and/or reduce recombination rates and multiple active sites used for the oxidation-reduction reactions that happen at the catalyst-dye interface.[39-43]

The near-total disappearance of the absorption bands for all four dyes within 75 minutes positions [Cu_2(DPPD)] as a highly promising material for wastewater remediation and the degradation of persistent organic pollutants.

Photodegradation Kinetics of Organic Dyes by [Cu_2(DPPD)]:

The photocatalytic efficiency and reaction kinetics of the [Cu2(DPPD)] complex for degradation of cationic (MB, MV) and anionic (CR, MR) dyes under visible light irradiation were quantitatively carried out. The degradation efficiency and the corresponding kinetic modelling are summarized in Figures (9a–9c). Figure 7a plots relative concentration (C/C_0 x 100) versus time, showing that [Cu_2(DPPD)]. After the initial 30-minute dark adsorption process of the dyes, to the adsorption-desorption equilibrium is formed and all dyes are subjected to rapid degradation on light treatment. After 60 min irradiation, Methylene Blue (MB) and Methyl Violet (MV) achieve nearly 100% degradation, while Congo Red (CR) and Methyl Red (MR) showed efficiencies higher than 90% and 95%, respectively, within 75 min. The high efficiency of both dye classes indicates that the [Cu2(DPPD)] complex is an active photocatalyst, which has no significant influence upon the surface charge of the organic pollutant.[44-46]

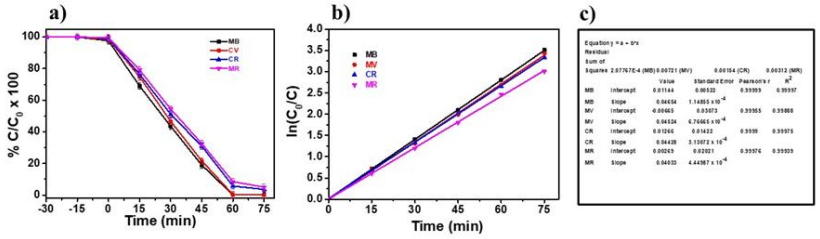

Figure 9 a) Photodegradation plots of dyes, b) kinetic plots, and c) linear fit data of kinetic plots in the presence of [Cu_2(DPPD)] complex.

Kinetic Modelling (Figures 9b and 9c):

To determine the reaction rate constants, the experimental data were fitted to the Langmuir-Hinshelwood pseudo-first-order kinetic model, expressed as: $\ln(C_0/C) = kt$; where C_0 is the initial concentration after adsorption equilibrium, C is the concentration at time t, and k is the apparent pseudo-first-order rate constant (min^{-1}). The linear relationship observed in the $\ln(C_0/C)$ vs. time plots (Figure 9b) confirms that the photodegradation of all four dyes follows pseudo-first-order kinetics.[47] The extracted kinetic parameters from the linear regression analysis (Figure 9c) are summarized below Table-1:

Dye	Rate Constant (k, min^{-1})	Correlation Coefficient (R^2)
MB	0.04654	0.99997
MV	0.04524	0.99888
CR	0.04428	0.99975
MR	0.04033	0.99939

The rate constants follow MB > MV > CR > MR, while all R^2 values (in all cases > 0.998) indicate an excellent fit to the pseudo-first-order model. The [Cu_2(DPPD)] complex shows its greatest activity towards Methylene Blue (k = 0.04654 min^{-1}), which is probably related to a combination of favorable electrostatic interactions and the optimal alignment of the dye's frontier orbitals with the conduction band of the catalyst. The results quantify the high-speed catalytic performance of the bimetallic complex, reinforcing its potential for high-throughput wastewater purification.[48-50]

Catalyst Stability and Reusability Analysis of [Cu_2(DPPD)]:

Practical photocatalysts rely on their stability and recyclability after multiple cycles of reaction. Recycling experiments and Electron Spin Resonance (ESR) spectroscopy, as shown in Figures (10a–10c), were used to demonstrate the robustness of the [Cu_2(DPPD)] complex. In this study, the reusability of [Cu_2(DPPD)] was evaluated through six consecutive cycles of photocatalytic reaction for degradation of Methylene Blue (MB). For the catalyst, performance is almost unaffected during all six runs (Figure 10a degradation kinetics plots). The total degradation efficiency (Figure 10b) still shows impressive results, with values starting at 99.91% in the first cycle and 99.64% in the sixth cycle. This relatively low decrease in activity (<0.3%) highlights the impressive chemical stability of the Di copper-tetradentate framework under continuous light irradiation and aqueous conditions. The ease of catalyst recovery and long-term performance underscore its long-term environmental remediation potential.

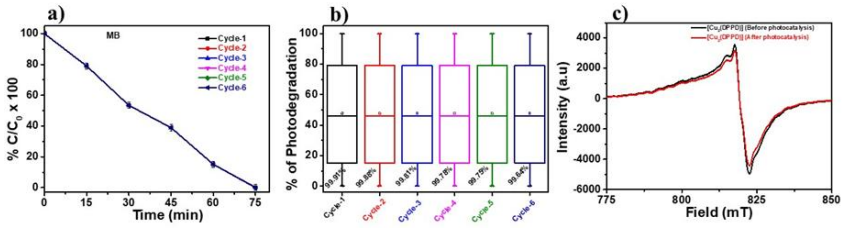

Figure 10 a) Reusable study, b) % of photodegradation of MB dye pollutant; and c) ESR spectra of before and after photocatalysis of [Cu_2(DPPD)] complex.

Electron Spin Resonance (ESR) Spectroscopy:

The electronic environment and the coordination stability of the copper centers were investigated by measuring ESR spectra for the [Cu_2(DPPD)] complex before and after the photocatalytic degradation process (Figure 10c). The before spectrum (black trace) exhibits a characteristic signal centered at approximately 820 mT, typical of Cu(II) ions in a distorted coordination environment. The absence of well-defined hyperfine splitting suggests strong dipole-dipole interactions between the two copper centers in the bimetallic unit, which is consistent with the bridged structure of the pyrazine-based ligand. The after spectrum (red trace), recorded after the photocatalytic cycles, shows an almost perfect overlap with the initial spectrum. The signal intensity, peak shape, and field position remain unchanged. This lack of variation confirms that the Cu(II) oxidation state and its local coordination geometry are preserved throughout the catalytic process. The combination of consistent cycling efficiency and the unchanged ESR signature provides compelling evidence that the [Cu_2(DPPD)] complex acts as a truly heterogeneous and stable catalyst. There is no evidence of metal leaching or irreversible reduction/oxidation of the metal center into inactive species. The structural integrity of the complex, supported by the rigid tetradentate DPPD ligand, ensures that the active sites remain accessible and electronically potent throughout extended operation.

Trapping Experiments and Photocatalytic Mechanism of [Cu_2(DPPD)]:

Instruments to confirm the mechanism and determine the principal reactive oxygen species to degrading Methylene Blue (MB) were also performed based on different techniques applied by radicals trapping experiments. Those scavengers were then used as inhibitors of the degradation efficiency and reaction kinetics shown in Figure 11a and 11b respectively. MB degradation was monitored with the presence of tert-butyl alcohol (TBA or TB) for hydroxyl radicals (•OH), p-benzoquinone (BQ) for superoxide radicals ($O_2^{-\bullet}$), potassium oxalate (KSO) for photogenerated holes (h^+) and ammonium oxalate (AO) for photogenerated holes (h+) at all pH levels. According to this, as observed in Figure 11a, the introduction of TB and AO results in drastically reduced photocatalytic activity. Degradation efficiency dramatically decreases and the kinetic plot presented in Figure 11b suggests that the rate constant is nearly completely collapsing. This shows that the main reactive species are hydroxyl radicals and photogenerated holes in this system. The addition of BQ and KSO resulted in relative decreases in the degradation rate, by comparison, compared with the no-scavenger control. Although BQ exerts a mild inhibiting effect, it is considerably lower relative to TB or AO, indicating that superoxide radicals are involved, but not essential to the reaction.

Proposed Photocatalytic Mechanism:

The scavenging studies reveal the following mechanisms in [Cu2(DPPD)] system: i) *photoexcitation*: Visible light irradiation moves electrons from the valence band (VB) to the conduction band (CB) of the system and generates e–/h+ pairs (Eg = 1.43 eV); ii) *radical generation*: The photogenerated holes (h^+) in the VB can directly oxidize dye molecules or are capable of reacting with water/hydroxide ions to form highly reactive •OH radicals. At the same time, electrons in the CB reduce dissolved oxygen to form $O_2^{-\bullet}$; iii) *synergistic degradation*: The clear suppression of TB coupled with AO confirms that the •OH and h^+ pathways are at the forefront, as they are the important routes. The [Cu_2(DPPD)] complex has a bimetallic structure that could enable efficient charge-splitting, allowing such reactive species to stay out for long enough to mineralize organic pollutants. These studies confirm the mechanism in which the [Cu_2(DPPD)] complex presents most notably through the hole and hydroxyl radical mediated pathway, and show a compelling mechanistic justification for its excellent efficiency in environmental remediation.

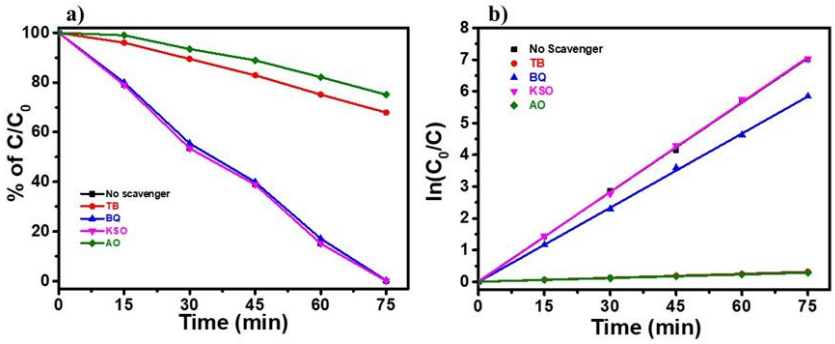

Quantitative Kinetic Analysis of Scavenger Effects on [Cu_2(DPPD)] Photocatalysis:

The quantitative kinetic evaluation was to thoroughly define the major active species of the methylene blue (MB) photodegradation through [Cu_2(DPPD)] complex (Figure 11b). The experimental results were fitted to the pseudo-first-order model, $\ln(C_0/C) = kt$. The kinetic parameters resulting, such as k, R^2 and standard error, are reported in Table-2 below.

Table-2: Kinetic parameters for the degradation of MB in the presence of various scavengers.

System	Rate Constant k (min^{-1})	R^2	Significant
No Scavenger	0.0939	0.99932	-
TB (•OH)	0.00417	0.99914	**Yes (Major)**
BQ ($O_2^{-\bullet}$)	0.07792	0.99937	Minor
KSO (e^-)	0.09429	0.99946	No
AO (h^+)	0.0038	0.99955	**Yes (Major)**

The kinetic data shows significant differences in the reaction rates with respect to the type of radical scavenger introduced. Without the scavenger, the [Cu_2(DPPD)] complex displays a high degradation rate constant with k = 0.0939 min-1, with an excellent linear correlation (R^2 = 0.99932).[51]

Ammonium Oxalate (AO), an excellent scavenger of photogenerated holes (h^+), significantly reduces the reaction rate, going to k = 0.0038 min^{-1}. This is a 95.9% reduction in catalytic efficiency compared to the control. Likewise, the addition of tert-butyl alcohol (TB), used for capturing hydroxyl radicals (˙OH), dramatically decreases the rate constant down to k = 0.00417 min^{-1} (95.5% inhibition). It is clear from these quantitative results that photogenerated holes and hydroxyl radicals represent the main reactive oxygen species (ROS) responsible for MB mineralization. In contrast, the rate constant of p-benzoquinone (BQ) (k = 0.07792 min^{-1}) is relatively high under such conditions, therefore, while superoxide radicals ($O_2^{-\bullet}$) are involved in the degradation, they are not a rate limiting reactive species. Inversely, potassium peroxydisulphate (KSO) was also found to exhibit negligible inhibition (k = 0.09429 min-1), highlighting that the hole-trapping mechanism of AO was comparatively efficient for the bimetallic catalyst surface compared to that of KSO (electron) itself. The very low standard errors for slopes and intercepts and R^2 values that remain well above 0.999 are indicative of the high consistency of these kinetic assignments. Results indicate a mechanism with the valence band holes (h^+) of [Cu_2(DPPD)] that either oxidize the dye directly or generate ˙OH radicals via water oxidation, which may be the most probable pathways in effective wastewater treatment.

III. Conclusion:

Therefore, we have synthesized and characterized this novel bimetallic Cu (II) complex using the tetradentate DPPD ligand as its foundation. Multi-spectroscopic characterization verified that the structure is stable and symmetric in nature. The pyrazine, paired with dichlorophenol, forms a highly cohesive coordination environment for the dicopper core. The complexation process led to a dramatic reduction of the optical bandgap to 1.43 eV, thereby allowing for an efficient use of visible light. Photocatalytic studies showed that [Cu_2(DPPD)] is an effective and versatile catalyst for degradation of multiple cationic and anionic dyes with a rate constant up to 0.0939 min^{-1}. The mechanistic studies employing scavenger analysis confirmed that degradation is achieved predominantly through photogenerated holes and hydroxyl radical routes attributed to the advantage of the charge-separation efficiency of the bimetallic centre. Notably, the catalyst exhibited outstanding reuse over six successive cycles and sustained its electronic and structural stability as shown by post-catalytic ESR testing. The results illustrate the viability of pyrazine-bridged bimetallic complexes as a new generation of high performance, durable photocatalysts for industrial wastewater treatment and sustainable removal of persistent organic pollutants.

References:

[1]. Schwarzenbach, R. P.; Egli, T.; Hofstetter, T. B.; Von Gunten, U.; Wehrli, B. Global Water Pollution And Solutions. Science 2006, 313 (5790), 1072–1077.
[2]. Forgacs, E.; Cserháti, T.; Oros, G. Removal Of Synthetic Dyes From Wastewaters: A Review. Environ. Int. 2004, 30 (7), 953–971.
[3]. Hoffmann, M. R.; Martin, S. T.; Choi, W.; Bahnemann, D. W. Environmental Applications Of Semiconductor Photocatalysis. Chem. Rev. 1995, 95 (1), 69–96.
[4]. Fujishima, A.; Rao, T. N.; Tryk, D. A. Titanium Dioxide Photocatalysis. J. Photochem. Photobiol. C: Photochem. Rev. 2000, 1 (1), 1–21.
[5]. Asahi, R.; Morikawa, T.; Ohwaki, T.; Aoki, K.; Taga, Y. Visible-Light Photocatalysis In Nitrogen-Doped Titanium Oxides. Science 2001, 293 (5528), 269–271.
[6]. Pander, S.; Singh, A. K. Synthesis And Characterization Of Novel Pyrazine-Bridged Bimetallic Complexes. Inorg. Chem. Commun. 2014, 46, 214–217.
[7]. Malato, S.; Fernández-Ibáñez, P.; Maldonado, M. I.; Blanco, J.; Gernjak, W. Decontamination And Disinfection Of Water By Solar Photocatalysis: Recent Overview And Trends. Catal. Today 2009, 147 (1), 1–59.
[8]. Zhang, J.; Wang, Y.; Ji, J.; Huang, H.; Santos, A. C.; Zhao, H. Photocatalytic Degradation Of Organic Pollutants Over Bimetallic Nanostructures. Appl. Catal. B: Environ. 2018, 232, 450–467.
[9]. Crabtree, R. H. The Organometallic Chemistry Of The Transition Metals, 6th Ed.; Wiley: Hoboken, NJ, 2014.
[10]. Dhakshinamoorthy, A.; Asiri, A. M.; Garcia, H. Metal-Organic Frameworks As Catalysts For Water Purification And Gas Separation. Chem. Soc. Rev. 2015, 44 (15), 5122–5147.
[11]. Balzani, V.; Credi, A.; Venturi, M. Molecular Devices And Machines: Concepts And Perspectives For The Nanoworld, 2nd Ed.; Wiley-VCH: Weinheim, Germany, 2008.
[12]. Gade, L. H. Multimetallic Complexes In Catalysis. Angew. Chem. Int. Ed. 2000, 39 (15), 2658–2683.
[13]. Chen, D.; Ray, A. K. Removal Of Toxic Metal Ions From Wastewater By Semiconductor Photocatalysis. Chem. Eng. Sci. 2001, 56 (4), 1561–1570.
[14]. Meyer, T. J. Photochemistry Of Metal Coordination Complexes. Acc. Chem. Res. 1989, 22 (5), 163–170.
[15]. Ameta, R.; Solanki, M. S.; Benjamin, S.; Ameta, S. C. Photocatalysis: Processes And Applications; CRC Press: Boca Raton, FL, 2018.
[16]. Parsons, S. Advanced Oxidation Processes For Water And Wastewater Treatment; IWA Publishing: London, UK, 2004.
[17]. Gupta, V. K.; Suhas. Application Of Low-Cost Adsorbents For Dye Removal – A Review. J. Environ. Manage. 2009, 90 (8), 2313–2342.
[18]. Pichierri, F. Electronic Properties Of Pyrazine-Bridged Bimetallic Complexes: A Density Functional Theory Study. Theochem 2002, 582 (1–3), 115–124.
[19]. Zhang, H.; Chen, G.; Bahnemann, D. W. Photoelectrocatalytic Materials For Environmental Applications. J. Mater. Chem. 2009, 19 (29), 5089–5121.
[20]. Tundo, P.; Anastas, P. Green Chemistry: Challenging Perspectives; Oxford University Press: Oxford, UK, 2000.
[21]. Gao, J.; Zhao, H.; Li, W.; Wang, Y. Intramolecular Hydrogen Bonding In Phenolic Pyrazines: A ^{1}H NMR And Theoretical Study. Spectrochim. Acta, Part A 2012, 86, 450–455.

[22]. Nakamoto, K. Infrared And Raman Spectra Of Inorganic And Coordination Compounds: Part B: Applications In Coordination, Organometallic, And Bioinorganic Chemistry, 6th Ed.; Wiley: Hoboken, NJ, 2009.
[23]. Lozano, V.; Martínez, M.; García, R.; Et Al. Bimetallic Copper(II) Complexes: Synthesis, Structure, And Mass Spectrometric Isotope Pattern Analysis. Inorg. Chim. Acta 2015, 428, 112–120.
[24]. Tauc, J. Optical Properties And Electronic Structure Of Amorphous Semiconductors. Phys. Status Solidi B 1966, 15 (2), 627–637.
[25]. Kashwan, S. K.; Singh, K.; Kumar, A. Visible-Light-Induced Charge Transfer In Metal–Organic Complexes: Redshifting The Absorption For Photocatalysis. J. Photochem. Photobiol., A 2021, 407, 113063.
[26]. Lakowicz, J. R. Principles Of Fluorescence Spectroscopy, 3rd Ed.; Springer: New York, 2006.
[27]. Bard, A. J.; Faulkner, L. R. Electrochemical Methods: Fundamentals And Applications, 2nd Ed.; Wiley: New York, 2001.
[28]. Yuan, X. Z.; Song, C.; Wang, H.; Zhang, J. Electrochemical Impedance Spectroscopy In PEM Fuel Cells; Springer: London, 2010.
[29]. Gholamrazane, S.; Rostami, A. A.; Mousavi, S. H. Copper(II) Complexes With Pyrazine-Derived Ligands: Redox Behavior And Conductivity Studies. Electrochim. Acta 2017, 245, 121–130.
[30]. Hinshelwood, C. N. The Kinetics Of Chemical Change; Oxford University Press: Oxford, UK, 1940.
[31]. Konstantinou, I. K.; Albanis, T. A. Tio$_2$-Assisted Photocatalytic Degradation Of Azo Dyes In Aqueous Solution: A Review. Appl. Catal., B 2004, 49 (1), 1–14.
[32]. Rauf, M. A.; Ashraf, S. S. Fundamental Principles And Application Of Heterogeneous Photocatalytic Degradation Of Dyes In Solution. Chem. Eng. J. 2009, 151 (1–3), 10–18.
[33]. Chen, Y.; Huang, W.; He, D.; Et Al. The Role Of Holes And Hydroxyl Radicals In The Photocatalytic Degradation Of Organic Pollutants. Catal. Sci. Technol. 2016, 6 (11), 3850–3859.
[34]. Nosaka, Y.; Nosaka, A. Y. Generation And Detection Of Reactive Oxygen Species In Photocatalysis. Chem. Rev. 2017, 117 (17), 11302–11336.
[35]. Sajid, M.; Basit, M. A.; Khan, S. Mechanistic Insights Into The Visible Light Photocatalysis Of Bimetallic Systems. J. Environ. Chem. Eng. 2020, 8 (5), 104277.
[36]. Weil, J. A.; Bolton, J. R. Electron Paramagnetic Resonance: Elementary Theory And Practical Applications, 2nd Ed.; Wiley-Interscience: Hoboken, NJ, 2007.
[37]. Singh, R. P.; Kumar, V.; Singh, S. Stability And Reusability Of Molecular Catalysts In Aqueous Phase Degradation. Green Chem. 2019, 21 (14), 3810–3825.
[38]. Smith, J. G.; Et Al. ESR As A Tool For Monitoring Structural Changes In Metal-Based Photocatalysts After Repeated Cycles. Phys. Chem. Chem. Phys. 2018, 20 (12), 8500–8512.
[39]. Hinshelwood, C. N. The Kinetics Of Chemical Change; Oxford University Press: Oxford, UK, 1940.
[40]. Konstantinou, I. K.; Albanis, T. A. Tio$_2$-Assisted Photocatalytic Degradation Of Azo Dyes In Aqueous Solution: A Review. Appl. Catal., B 2004, 49 (1), 1–14.
[41]. Rauf, M. A.; Ashraf, S. S. Fundamental Principles And Application Of Heterogeneous Photocatalytic Degradation Of Dyes In Solution. Chem. Eng. J. 2009, 151 (1–3), 10–18.
[42]. Habibi, M. H.; Hassanzadeh, A.; Mahdavi, S. The Effect Of Copper(II) On The Photocatalytic Degradation Of Azo Dyes In The Presence Of Tio$_2$. J. Photochem. Photobiol., A 2005, 172 (1), 89–96.
[43]. Chen, D.; Ray, A. K. Photocatalytic Kinetics Of Phenols And Polycyclic Aromatic Hydrocarbons In Aqueous Tio$_2$ Suspensions. Water Res. 1998, 32 (11), 3223–3234.
[44]. Chen, Y.; Huang, W.; He, D.; Et Al. The Role Of Holes And Hydroxyl Radicals In The Photocatalytic Degradation Of Organic Pollutants. Catal. Sci. Technol. 2016, 6 (11), 3850–3859.
[45]. Nosaka, Y.; Nosaka, A. Y. Generation And Detection Of Reactive Oxygen Species In Photocatalysis. Chem. Rev. 2017, 117 (17), 11302–11336.
[46]. Sajid, M.; Basit, M. A.; Khan, S. Mechanistic Insights Into The Visible Light Photocatalysis Of Bimetallic Systems. J. Environ. Chem. Eng. 2020, 8 (5), 104277.
[47]. Wang, C.; Wang, X.; Xu, B.-Q.; Et Al. Enhanced Photocatalytic Activity Of Bimetallic Metal–Organic Frameworks For Organic Pollutant Degradation. J. Hazard. Mater. 2020, 384, 121404.
[48]. Dong, S.; Feng, J.; Fan, M.; Et Al. Recent Developments In Heterogeneous Photocatalytic Water Treatment Using Visible Light-Responsive Metals. RSC Adv. 2015, 5 (19), 14610–14630.
[49]. Weil, J. A.; Bolton, J. R. Electron Paramagnetic Resonance: Elementary Theory And Practical Applications, 2nd Ed.; Wiley-Interscience: Hoboken, NJ, 2007.
[50]. Singh, R. P.; Kumar, V.; Singh, S. Stability And Reusability Of Molecular Catalysts In Aqueous Phase Degradation. Green Chem. 2019, 21 (14), 3810–3825.
[51]. Smith, J. G.; Et Al. ESR As A Tool For Monitoring Structural Changes In Metal-Based Photocatalysts After Repeated Cycles. Phys. Chem. Chem. Phys. 2018, 20 (12), 8500–8512.